ISSN(Online): 2319-8753
ISSN (Print): 2347-6710

International Journal of Innovative Research in Science, Engineering and Technology

(An ISO 3297: 2007 Certified Organization)

Website: www.ijirset.com

Vol. 6, Issue 8, August 2017

Self-Tuned NFC and Adaptive Torque Hysteresis-Based DTC Scheme for IM Drive

M.Chanakya[1], S.Sridhar[2]

PG Student [Power Industrial Drives], Dept. of EEE, JNTU Ananthapur, AP, India[1]

Assistant professor, Dept. of EEE, JNTU Ananthapur, AP, India[2]

ABSTRACT: This project presents a simplified self-tuned Sugeno type neuro-fuzzy controller (NFC)-based direct torque control (DTC) scheme for induction motor (IM) drive. A simple tuning algorithm is developed based on the reference and actual acceleration of the motor. The online tuning strategy adjusts the parameters of the consequent layer of the NFC in order to minimize the square of the error between the actual and the reference acceleration of the motor. In a conventional DTC scheme, the band limits of flux and torque hysteresis controllers remain fixed, and hence, the torque and flux ripples are high. In order to minimize the torque ripples of the IM, the hysteresis band limits are adjusted online for the torque hysteresis controller. Thus, the proposed NFC is used to achieve high dynamic performance of the drive, and the variable hysteresis controller is used to reduce the steady-state torque ripple.

KEYWORDS: Direct torque control, induction motor, neuro fuzzy control, speed control torque ripple.

I. INTRODUCTION

IN CLASSICAL control systems, the accuracy of the control is highly dependent on plant mathematical models [1].The majority of the models are complex, parameter dependent and based on many assumptions for simplicity. These assumptions introduce the proportional amount of inaccuracy in the model. Conclusively, the model-based controllers, like a classical proportional–integral (PI) controller, are slow adapting to speed changes, load disturbances, and parameter variations [2]–[5]. The major advantage of artificial intelligent controllers (AICs) is that they need only the approximate mathematical model of the system for their working. The ideal behavior of AIC is its capability to learn, recall, and generalize from training patterns or data like the human brain [6], [7]. The use of advanced electronics has made it possible to implement the complex controllers by using a powerful microprocessor. There are mainly three types of AICs which include fuzzy logic, neural network, and their hybrid neuro-fuzzy network. The main advantages of AICs are that their designs do not need any exact system mathematical model and they can handle any system nonlinearities and uncertainties.

However, the design accuracy of a pure fuzzy logic controller (FLC) is highly dependent on expert knowledge. Moreover, for high performance dynamic control, it needs a laborious trial-and-error technique for the final selection of the membership functions and rules [8]. On the other hand, it is very difficult to achieve the training data required for a pure artificial neural network (ANN) that can handle all the operating modes of the system [9], [10].

The neuro-fuzzy controller (NFC) utilizes the transparent linguistic representation of a fuzzy system with the learning ability of ANNs. It enables the system to be adaptive and requires minimum human intervention for the tuning [10]. To the best of the authors' knowledge, no major work has been reported on the application of self-tuned NFC for online adaptive direct torque control (DTC)-based induction motor (IM) drive. In order to improve the dynamic speed response, the authors have used a PI controller for the steady state and a FLC for the transient state. The switching mechanism is based on the magnitude of the speed error. The threshold of the switching limit for the two controllers is based on the sampling frequency and the type of the FLC used. These factors make the transition of switching very complicated and restrict the application of this hybrid controller only to a specific drive under specific conditions. Furthermore, the PI controller is used in steady state, which is highly dependent on motor parameters and system disturbances.

The majority of the reported works are related to replace the DTC table and/or hysteresis comparators by either neural network or fuzzy logic-based algorithms [11].Therefore, in this paper, a stand-alone Takagi–Sugeno–Kang (TSK)-type

ISSN(Online): 2319-8753
ISSN (Print): 2347-6710

International Journal of Innovative Research in Science, Engineering and Technology

(An ISO 3297: 2007 Certified Organization)

Website: www.ijirset.com

Vol. 6, Issue 8, August 2017

self-tuned NFC is developed to improve the dynamic speed response of the IM drive. Ideally, the target is to keep the torque ripples constant within fixed limits. Then, the proposed NFC-based DTC scheme is implemented in real time using the DSP board DS1104 for a prototype 1-hp motor. The effectiveness of the proposed drive is verified at different dynamic operating conditions in both simulation and experiment. The proposed controller is found robust to parameter sensitivity and also has a learning/training algorithm to adapt with system uncertainties.

II. MODELING OF IM FOR DTC

The mathematical model of an IM in the stationary reference frame can be written as

$$\begin{bmatrix} v_{s\alpha} \\ v_{s\beta} \\ 0 \\ 0 \end{bmatrix} = \begin{bmatrix} R_S + pL_s & 0 & pL_m & 0 \\ 0 & R_S + pL_s & 0 & pL_m \\ pL_m & P\omega_m L_m & R_r + pL_r & P\omega_m L_r \\ -P\omega_m L_m & pL_m & -P\omega_m L_r & R_r + pL_r \end{bmatrix} + \begin{bmatrix} i_{s\alpha} \\ i_{s\beta} \\ i_{rd} \\ i_{rq} \end{bmatrix}. \quad (1)$$

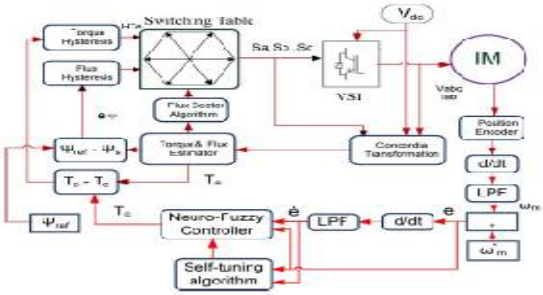

Fig. 1. NFC-based DTC scheme for IM drive.

The proposed NFC-based DTC scheme for IM drive is shown in Fig. 1. The output voltage of a three-phase voltage source inverter (VSI) or the input to the stator of the IM is given by

$$V_{sa} = \frac{V_{dc}}{3}(2S_a - S_b - S_c) \quad (2\text{-a})$$

$$V_{sb} = \frac{V_{dc}}{3}(2S_b - S_c - S_a) \quad (2\text{-b})$$

$$V_{sc} = \frac{V_{dc}}{3}(2S_c - S_a - S_b). \quad (2\text{-c})$$

The real and imaginary parts of the stator voltage vector are obtained by using the Concordia transformation as

$$\begin{bmatrix} V_{s\alpha} \\ V_{s\beta} \end{bmatrix} = \begin{bmatrix} 1 & 1/2 & 1/2 \\ 0 & \sqrt{3}/2 & \sqrt{3}/2 \end{bmatrix} \begin{bmatrix} V_{sa} \\ V_{sb} \\ V_{sc} \end{bmatrix}. \quad (3)$$

The motor-developed torque is given by

$$T_e = \frac{3}{2}P[\psi_{s\alpha} I_{s\beta} - \psi_{s\beta} I_{s\alpha}]. \quad (4)$$

The stator flux angle, flux vector, and its components are given by

$$\theta_s = \tan^{-1}(\psi_{s\beta}/\psi_{s\alpha}) \quad (5.a)$$

ISSN(Online): 2319-8753
ISSN (Print): 2347-6710

International Journal of Innovative Research in Science, Engineering and Technology

(An ISO 3297: 2007 Certified Organization)

Website: www.ijirset.com

Vol. 6, Issue 8, August 2017

$$\psi_s = \sqrt{\psi_{s\alpha}^2 + \psi_{s\beta}^2} \quad (5.b)$$

$$\psi_{s\alpha} = \int (V_{s\alpha} - R_s I_{s\alpha}) dt \quad (6.a)$$

$$\psi_{s\beta} = \int (V_{s\beta} - R_s I_{s\beta}) dt. \quad (6.b)$$

The well-known problems associated with the real-time implementation of the pure integral in (6.a) and (6.b) are easily overcome by modifying the integral as follows [26]:

$$\psi_{s\alpha} = \int \{[1 - j\lambda \text{sign}(w)](V_{s\alpha} - R_s I_{s\alpha}) - \lambda |w| \psi_{s\alpha}\} dt \quad (7.a)$$

$$\psi_{s\beta} = \int \{[1 - j\lambda \text{sign}(w)](V_{s\beta} - R_s I_{s\beta}) - \lambda |w| \psi_{s\beta}\} dt. \quad (7.b)$$

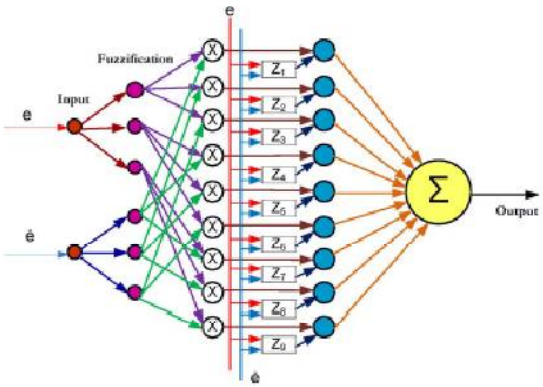

Fig. 2. General structure of conventional TSK-type NFC.

Based on the simulation and experimental tests, the value of λ is optimized to 3.1.The two digits produced by the hysteresis comparators and one digit produced by the flux position are collectively used to trigger the switches of the VSI which selects the appropriate voltage vector by using the classical DTC lookup table. The block diagram of the proposed NFC-based DTC scheme incorporating the hysteresis band adaptation for IM drive is shown in Fig. 1.

III. DEVELOPMENT OF NFC

A. General Structure of a TSK-Type NFC: The general structure of a TSK-type NFC, with five layers, used for the DTC-based IM drive is shown in Fig. 2 [28]. However, the design of the NFC used in this paper is totally different from the one in [28] in terms of the membership function selection and tuning algorithm. In this paper, the membership functions are piecewise linear, whereas in [28], those are sigmoidal and Gaussian functions. In this paper, for tuning purpose, a different type of reference acceleration function is selected than the one used in [28].Moreover, the overall control schemes used in this paper and in [28] are totally different as the NFC in [28] is used for the conventional vector control scheme and the NFC in this paper is used for the DTC of a different size IM.

The speed error "*e*" and change in speed error "$e^{\cdot}$" are the inputs, and *Tc* is the output of the NFC. Each linguistic variable consists of three membership functions (mfs) shown by math dotted lines in Fig. 3. The Gaussian membership function is used for mf-ZE (zero), and the sigmoid membership function is used for both mf-PS (positive small) and mf-NE (negative). This combination naturally produces nine rules for the NFC. The excellence of the exponential function is that it changes slowly as it approaches to the saturation values, and in the middle, the slope is almost linear. This is one of the desired properties of the speed controller. However, there is a tradeoff as the value of

ISSN(Online): 2319-8753
ISSN (Print): 2347-6710

International Journal of Innovative Research in Science, Engineering and Technology

(An ISO 3297: 2007 Certified Organization)

Website: www.ijirset.com

Vol. 6, Issue 8, August 2017

the exponential function is calculated by the processor using some algorithms based on the approximation of some infinite series, e.g., the Taylor series [29]. Moreover, the

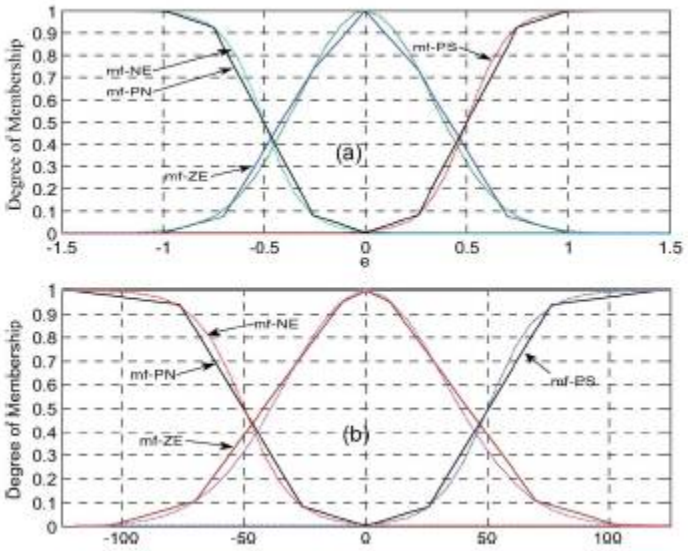

Fig. 3. Membership functions for linguistic input variables. (a) "*e*." (b) "*ė*."

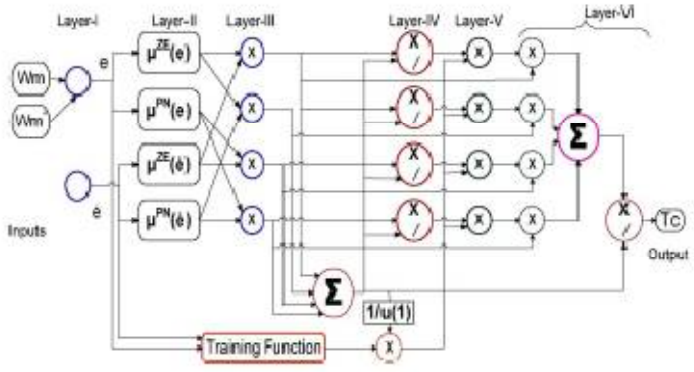

Fig. 4. Structure of the proposed Sugeno-type NFC.

exponential function value is nonzero for the whole operating range of the controller input variables. It means that all the nine rules are nonzero all the time, even though their values are so small that they have no significance for the controller. These factors introduce a high volume of computational burden on the processor. This may cause the processor for real-time implementation to overrun. Consequently, to run the controller smoothly, it needs to increase the sampling time, which may ruin the whole advantage of the exponential function, and the controller becomes useless.

B. Detailed Design of the Proposed TSK-Type NFC

The structure of the proposed specific NFC is shown in Fig. 4. The function of each layer of the proposed NFC is briefly described as follows.

1) *Layer-I*: In the first layer, the normalized speed error and
the motor acceleration, i.e., rate of change of actual speed, are calculated. The output of the first layer, which is the input to the second layers is given as

ISSN(Online): 2319-8753
ISSN (Print): 2347-6710

International Journal of Innovative Research in Science, Engineering and Technology

(An ISO 3297: 2007 Certified Organization)

Website: www.ijirset.com

Vol. 6, Issue 8, August 2017

$$e = O_1^I = \frac{\omega_m^* - \omega_m}{\omega_m^*} \quad (8.a)$$

$$\dot{e} = O_2^I = \frac{\omega_m[n] - \omega_m[n-1]}{T_s}. \quad (8.b)$$

The letter "*O*" represents the output of the layer, and its subscript and superscript represent the member function number and layer number, respectively. *Ts* is the sampling period, and $\omega m[n]$ and $\omega m[n-1]$ stand for the present and the previous sample of the actual speed, respectively.

2) *Layer-II*: This is the fuzzification layer. Each crisp input value is fuzzified by using its membership functions. In the proposed controller, three membership functions (strategically, it can be seen as two membership functions due to symmetry) are selected for both the inputs as

shown in Fig. 3. In order to reduce the computational burden, the exponential membership function are approximated by linear functions as shown by solid lines in Fig. 3. Although there are different linear segments of the membership function, at each operating point, only one segment calculation is required. Thus, it saves a lot of calculation in fuzzification. It is clear from Fig. 3 that both the mfs μZE(e) and μZE($\dot{e}$) are symmetric about the origin. Also, the mfs μPS(e) and μNE(e) are mirror images of each other. The case with linguistic variable "$\dot{e}$" mfs is similar. Choosing the absolute crisp values of the variables "e" and "$\dot{e}$" makes the case simpler and reduces the mfs for each variable to two instead of three. The node equations for membership functions in Layer-II are given as

$$O_1^{II} = \mu^{PN}(e) \begin{cases} 0.32|e| & 0 \le |e| \le 0.26 \\ 1.72|e| - 0.364 & 0.26 < |e| \le 0.75 \\ 0.3|e| + 0.7 & 0.75 < |e| \le 1 \\ 1, & |e| > 1 \end{cases} \quad (9.a)$$

$$O_2^{II} = \mu^{ZE}(e) \begin{cases} 1 - \frac{27}{26}|e| & 0 \le |e| \le 0.26 \\ 1.12 - 1.49|e| & 0.26 < |e| \le 0.75 \\ 0.25\,(1 - |e|) & 0.75 < |e| \le 1 \\ 0, & |e| > 1 \end{cases} \quad (9.b)$$

$$O_4^{II} = \mu^{ZE}(\dot{e}) \begin{cases} 1 - 0.005|e| & 0 \le |e| \le 10 \\ 0.81 - 0.014|e| & 10 < |e| \le 70 \\ 0.315 - 0.003|e| & 70 < |e| \le 105 \\ 0, & |e| > 105. \end{cases} \quad (9.d)$$

The parameters used in (9) have been derived based on their equivalent continuous complex exponential functions shown in Fig. 3. In this case, the best suitable parameters are found in simulation by the trial-and-error procedure.

3) *Layer-III*: This is the first step of fuzzy rule evaluation. The rule may be evaluated by any appropriate method like minimum, product, or height. In the proposed NFC, the product method is chosen to implement the "AND" logic. The output of each node in this layer gives the firing strength of the corresponding rule. Since there are two inputs with each having two membership functions,

$$O_3^{II} = \mu^{PN}(\dot{e}) \begin{cases} 3.07 * 10^{-3}|e| & 0 \le |e| \le 26 \\ 0.017|e| - 0.366 & 26 < |e| \le 76 \\ 1.37 * 10^{-3}|e| - 1043 & 76 < |e| \le 120 \\ 1, & |e| > 120 \end{cases} \quad (9.c)$$

ISSN(Online): 2319-8753
ISSN (Print): 2347-6710

International Journal of Innovative Research in Science, Engineering and Technology

(An ISO 3297: 2007 Certified Organization)

Website: www.ijirset.com

Vol. 6, Issue 8, August 2017

therefore, four nodes are assigned in this layer covering all possible cases. Hence, in the proposed NFC, the maximum active rules at any time reduce to four instead of nine as in the conventional NFC [28]. The node equation in Layer-III can be specified as

$$O_i^{III} = W_i = \prod_{j=1,2}^{k=3,4} (O_j^{II} * O_k^{II}) \qquad (10)$$

where *OII j* and *OII k* are fuzzy numbers produced by the fuzzification of linguistic variables "*e*" and "*e*˙," respectively.
4) *Layer-IV*: The normalized firing strength of each rule is determined in this layer. This is the second and the final step of fuzzy rule evaluation. The node equation in this layer can be specified as

$$O_i^{IV} = \overline{W_i} = \frac{W_i}{\sum W_i} \qquad (11)$$

where $\overline{wi}$ is the normalized firing strength of the *i*th rule.5) *Layer-V (consequent layer)*: The parameters in this layer are called the consequent parameters. The crisp values of the variable are used in this step instead of their fuzzified values. This is the preference of Sugeno-type NFC over Mamdani which uses fuzzified values of the variable and needs defuzzification at the end [1]. Thus, the computational burden in the Sugeno-type NFC is less than that of the Mamdani-type NFC. The output of each node in this layer can be specified as

$$O_i^V = Z_i^{IV} * O_i^{IV} \qquad (12)$$

where ZIV *i* is the adaptive weight factor for the *i*th node. It is a function of crisp values of variables "*e*" and "*de*" and is obtained in this paper through the training function that will be explained in Section-III(C).
6) *Layer-VI*: This is the last step for the calculation of output of the controller. The output of this layer can be specified as

$$O^{VI} = \sum (O_i^{III} * O_i^V) \Big/ \sum O_i^{III}. \qquad (13)$$

Plugging (12) into (13), the command torque (final output of the controller) can be rewritten as

$$T_c = O^{VI} = \sum (O_i^{III} * Z_i^{IV} * O_i^{IV}) \Big/ \sum O_i^{III}. \qquad (14)$$

This is the command torque of the DTC scheme for the IM drive. This torque forces the motor to follow the command speed.

C. Tuning Algorithm for the Controller

Under varying dynamic conditions of the IM drive, it is almost impossible to determine the NFC desired output *Tc*. Ideally, it requires a unique operating curve for the motor under each dynamic condition even for the same speed error. Obviously, under different operating conditions, it requires a

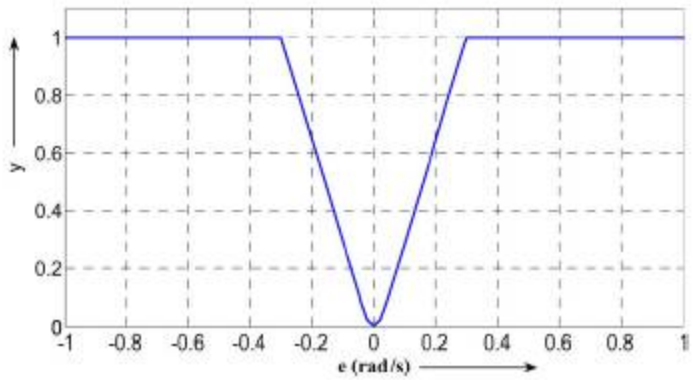

Fig. 5. Reference acceleration for controller, *y*.

ISSN(Online): 2319-8753
ISSN (Print): 2347-6710

International Journal of Innovative Research in Science, Engineering and Technology

(An ISO 3297: 2007 Certified Organization)

Website: www.ijirset.com

Vol. 6, Issue 8, August 2017

kind of online self-tuning method for the controller to work properly. The tuning algorithm for the consequent parameters ZIV *i* can be developed using a reinforcement signal "*r*" which is based on the difference between the reference acceleration "*y*" and the actual acceleration (*dω/dt*) of the motor. The reinforcement signal is utilized to generate the control action to produce the desired speed response. The reference acceleration model "*y*" is designed as shown in Fig. 5. The corresponding mathematical model is given as follows:

$$y=\begin{cases} 0.99|e|*K_1*\text{sign}(e), & 0\le|e|\le 0.02 \\ (2.854|e|-0.0373)*K_1*\text{sign}(e), & 0.02<|e|\le 0.04 \\ (3.3|e|-0.055)*K_1*\text{sign}(e), & 0.04<|e|\le 0.32 \\ K_1*\text{sign}(e), & |e|>0.32 \end{cases} \quad (15)$$

$$E=\frac{1}{2}r^2=\frac{1}{2}\left(y-\frac{d\omega_m}{dt}\right)^2=\frac{1}{2}\left(y-O_2^I\right)^2. \quad (16)$$

where *K*1 is a gain and the operator "sign" yields the sign of the error signal "*e*." The error between the reference and the actual acceleration of the IM for the controller may be defined as

$$O_2^I=K_2*T_c=K_2*O^{VI} \quad (17)$$

The consequent parameter ZIV *i* in the fifth layer is updated by the controller in each sampling time to converge this acceleration error to zero since the IM acceleration is proportional to the developed torque or vice versa. Therefore, it may be summarized as where *K*2 is the proportionality constant. Combining (14) and (15), the updated law can be expressed as

$$Z_i^{IV}(n)=Z_i^{IV}(n-1)-\eta'\left(\frac{\delta E}{\delta Z_i^V}\right)\frac{O_i^{III}}{\sum O_j^{III}}=\eta'\left(\frac{\delta E}{\delta O_2^I}\right)\frac{\delta O_2^I}{\delta Z_i^V}. \quad (18)$$

Using (13), (16), and (17), the self-learning algorithm can be redefined as

$$Z_i^{IV}(n)=Z_i^{IV}(n-1)+\eta\left(y-\frac{d\omega_m}{dt}\right)\frac{O_i^{III}}{\sum O_j^{III}} \quad (19)$$

where $\eta = k \square \eta\_$ is the learning rate which is set to 0.001 in this paper. The value of η may be obtained by trial-and-error method or self-tuning method. For the proposed controller, the value

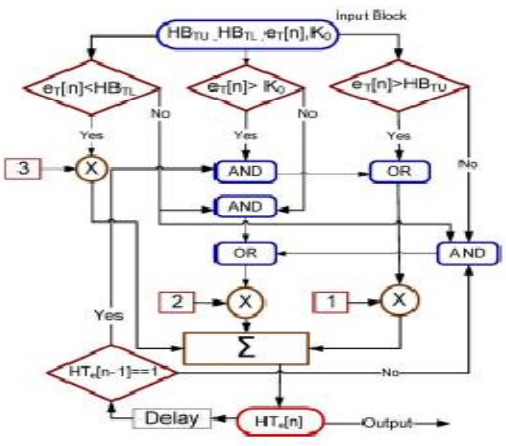

Fig. 6. Proposed three-level torque hysteresis comparator.

ISSN(Online): 2319-8753
ISSN (Print): 2347-6710

International Journal of Innovative Research in Science, Engineering and Technology

(An ISO 3297: 2007 Certified Organization)

Website: www.ijirset.com

Vol. 6, Issue 8, August 2017

of η is obtained by trial-and-error method. Smaller values of training rate η results in small acceleration and takes a very long time to reach the reference speed; sometimes, the controller
may never even be able to get the desired targeted speed. On the other hand, larger values of η causes rapid acceleration but at the cost of big torque and current ripples, which cause extra power loss due to harmonic current and motor vibration.

IV. DESIGN OF TORQUE HYSTERESIS COMPARATOR

The algorithm for the proposed three-level torque hysteresis comparator is shown in Fig.4. Digits 1, 2, and 3 are used for the digits 1, 0, and −1 of the conventional DTC table, as the output of the torque hysteresis comparator, respectively. HTe[n] and HTe[n − 1] are the current and previous samples of the output digits produced by the torque hysteresis comparator. For instance, the output of the torque hysteresis comparator will be 1 if either eT [n] > HBTU or eT [n] > K0 AND HTe[n − 1] == 1. The torque error eT is the difference between the command and actual values of the IM torque. The basic idea is to use the zero voltage vector for the reduction of the torque and to avoid the application of the negative voltage vector to the possible limit.

This reduces the negative slope of the developed torque which tends to reduce the switching rate from the inverter and, hence, to reduce the torque ripples in the negative torque region. However, in order to improve the system dynamics under varying loading conditions and to avoid big positive torque ripples, the proposed hysteresis regulator applies the negative voltage vector a small interval before HBTL at point K0. This margin is of critical nature. The value for K0 and its distance from HBTL are determined on the basis of simulation results of system characteristics under varying load and speed conditions. The bandwidth of hysteresis is not constant in this scheme. The control of torque ripple is achieved through the dynamic change of the hysteresis band limits. The required change (ΔHBT) is evaluated by using the algorithm shown in Fig. 5.

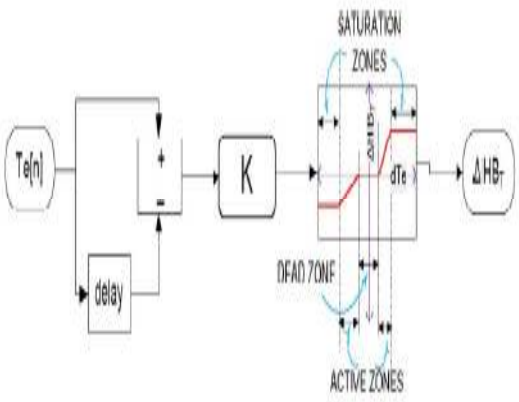

Fig. 5. Proposed bandwidth adaptation algorithm.

The term dTe is the slope of the torque ripple and is given by

$$dT_e = (T_e[n] - T_e[n-1]) . \quad (20)$$

Net upper and lower band limits of the torque hysteresis controller are given by

$$HB^n_{TU} = HB_{TU} - K_U * \Delta HB_T \quad (21)$$
$$HB^n_{TL} = HB_{TL} + K_L * \Delta HB_T . \quad (22)$$

The amount of positive torque ripple varies inversely with the load and speed. The reverse is the case for the negative torque slope. Once again, the width of three zones is based on simulation results of the system response under variable conditions. The most effective parts are the active zones. The change in current bandwidth is predicted on the

ISSN(Online): 2319-8753
ISSN (Print): 2347-6710

International Journal of Innovative Research in Science, Engineering and Technology

(An ISO 3297: 2007 Certified Organization)

Website: www.ijirset.com

Vol. 6, Issue 8, August 2017

basis of the change in the estimated torque in the previous sampling time. The net bandwidth is selected in such a way that the torque peaks (both positive and negative around the set position) remain near the boundaries (HBTU,HBTL) within permissible small deviations. Due to the limitation imposed by the maximum switching rate of the VSI, it is almost impossible that the peaks of torque always touch the maximum defined limits.

V. SIMULATION RESULTS

Proposed NFC:

Case.1:

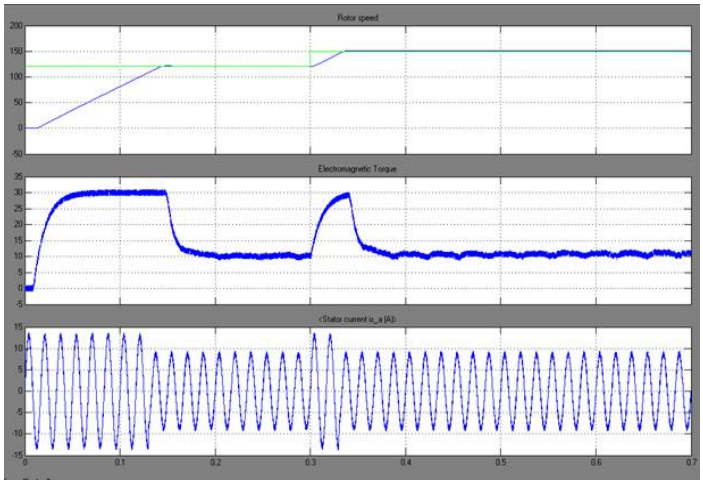

Case.2:

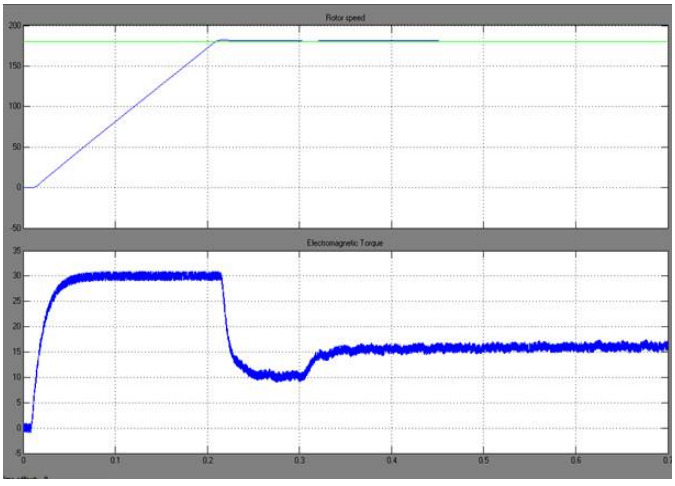

ISSN(Online): 2319-8753
ISSN (Print): 2347-6710

International Journal of Innovative Research in Science, Engineering and Technology

(An ISO 3297: 2007 Certified Organization)

Website: www.ijirset.com

Vol. 6, Issue 8, August 2017

Case.3:

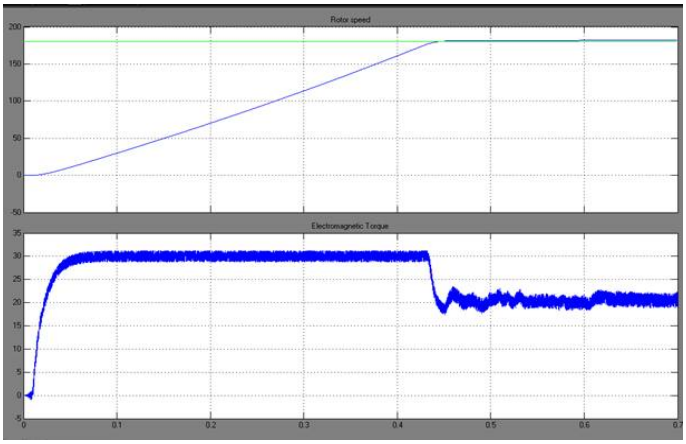

Fig6: Developed torque, stator current and speed responses of the IM drive for a step change.

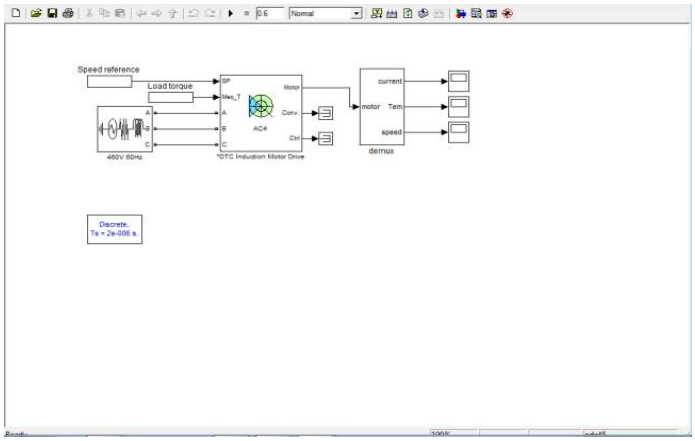

Fig7: simulation diagram of adaptive torque Hysteresis-based DTC scheme for IM drive.

ISSN(Online): 2319-8753
ISSN (Print): 2347-6710

International Journal of Innovative Research in Science, Engineering and Technology

(An ISO 3297: 2007 Certified Organization)

Website: www.ijirset.com

Vol. 6, Issue 8, August 2017

Proportional DTC:

case.1.

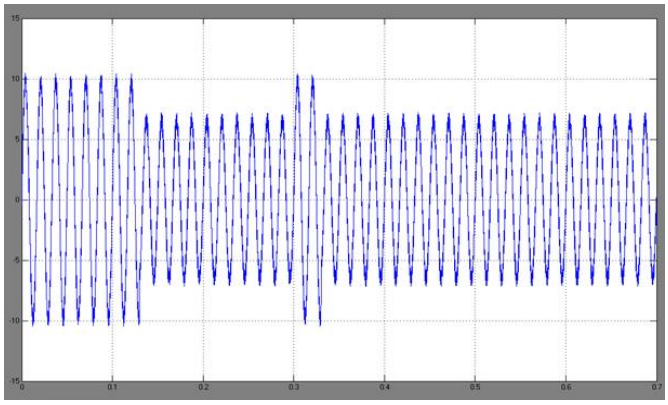

Fig.8. Stator "a" phase current of the IM drive for step change in speed fro120 to 150 rad/s at 50%of rated load. (a) Conventional DTC

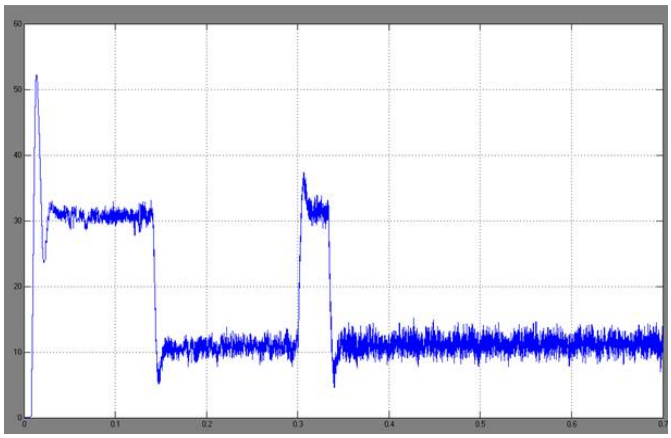

Fig.9. Developed torque of the IM drive for step change in speed from 120 to 150 rad/s at 50% of rated load. (a) Conventional DTC

ISSN(Online): 2319-8753
ISSN (Print): 2347-6710

International Journal of Innovative Research in Science, Engineering and Technology

(An ISO 3297: 2007 Certified Organization)

Website: www.ijirset.com

Vol. 6, Issue 8, August 2017

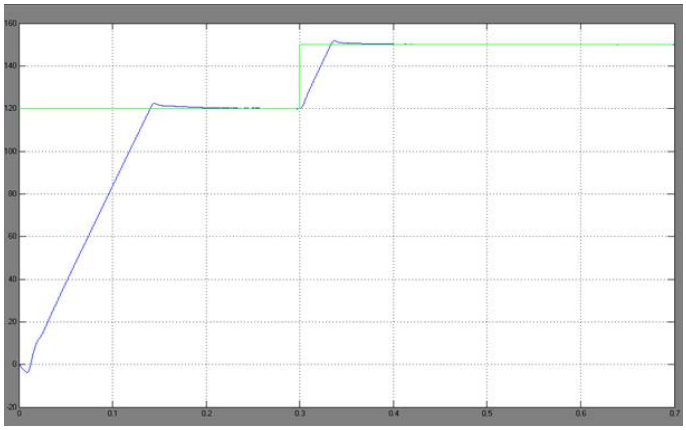

Fig.10. Speed responses of the IM drive (with zoom-in view of the encircled part of response) at rated load and rated speed of 180 rad/s. (a) Conventional DTC.

Case.2

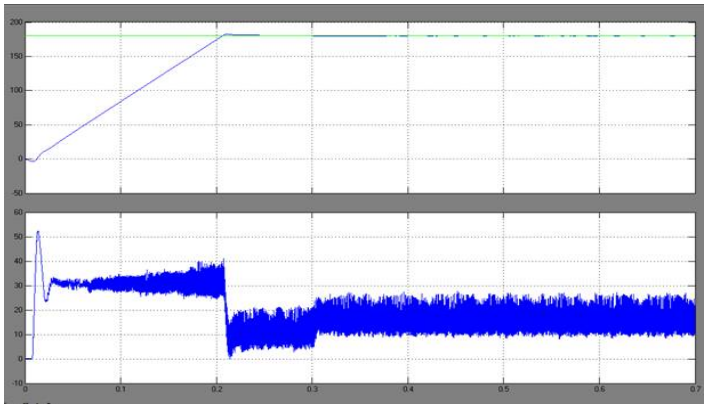

Fig:11. Developed torque, stator current and speed responses of the IM drive for a step change.

Case.3

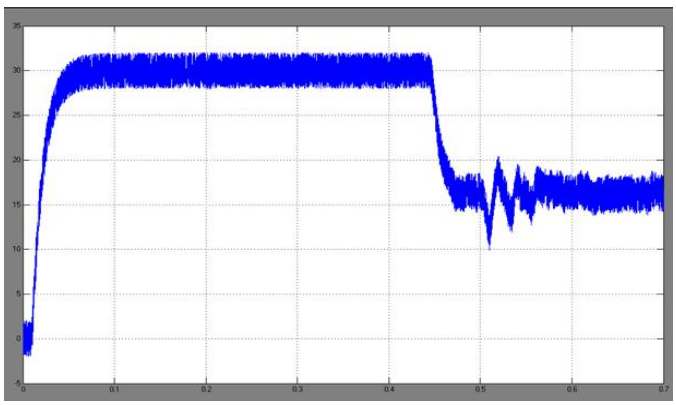

Fig.12.Developed torque of the IM drive for step change in speed from 120 to 150 rad/s at 50% of rated load. (a) Conventional DTC

ISSN(Online): 2319-8753
ISSN (Print): 2347-6710

International Journal of Innovative Research in Science, Engineering and Technology

(An ISO 3297: 2007 Certified Organization)

Website: www.ijirset.com

Vol. 6, Issue 8, August 2017

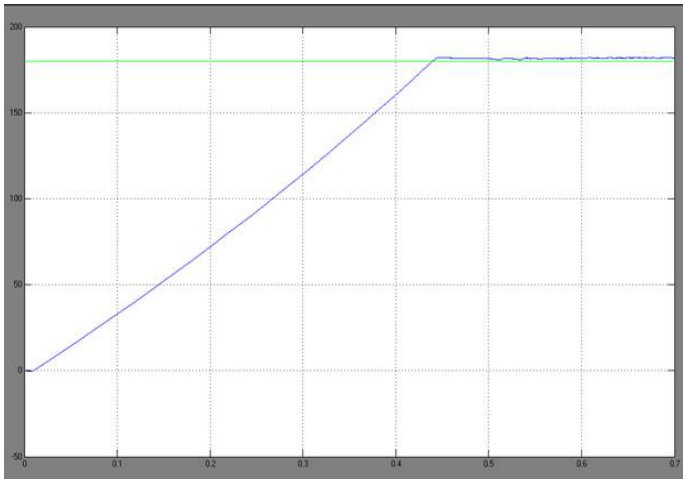

Fig.13. Speed responses of the IM drive (with zoom-in view of the encircled part of response) at rated load and rated speed of 180 rad/s. (a) Conventional DTC.

VI. CONCLUSION

A novel NFC-based DTC scheme incorporating a variable band torque hysteresis comparator for IM drive has been presented in this paper. The NFC is used to improve the dynamic speed response of the drive. The NFC is designed in such a way that the computation burden is reduced and hence suitable for real-time application. The proposed NFC and DTC-based IM drive has been successfully implemented in real time using the DSP board DS1104 for a laboratory 1-hp IM. A performance comparison of the proposed NFC and DTC-based IM drive with a conventional DTC-based IM drive has also been provided in both simulation and experiment. Comparative simulation and experimental results show that the proposed self-tuned NFC and variable band hysteresis comparator-based DTC scheme for IM drive is superior to the conventional DTC scheme in terms of settling time, speed, and torque ripples.

REFERENCES

[1]P. Vas, *Artificial-Intelligence-Based Electrical Machines and Drives*. London, U. K.: Oxford Univ. Press, 1999.
[2] S. V. Jadhav, J. Srikanth, and B. N. Chaudhari, "Intelligent controllers applied to SVM-DTC based induction motor drives: A comparative study," in *Proc. IEEE Power India Int. Joint Conf. Power Electron., Drives Energy Syst.*, Dec. 2010, pp. 1–8.
[3] H. A. F. Mohamed and W. P. Hew, "A fuzzy logic vector control of induction motor," in *Proc. IEEE TENCON*, Aug. 2002, vol. 3, pp. 324–328.
[4] F. Barrero, A. González, A. Torralba, E. Galván, and L. G. Franquelo, "Speed control of induction motors using a novel fuzzy sliding-mode structure," *IEEE Trans. Fuzzy Syst.*, vol. 10, no. 3, pp. 375–383, Jun. 2002.
[5] M. N. Uddin, Z. R. Huang, and M. M. I. Chy, "A simplified selftuned neuro-fuzzy controller based speed control of an induction motor drive," in *Proc. IEEE Power Eng. Soc. Gen. Meet.*, Tampa, FL, USA 2007, pp. 1–8.
[6]L. Zhang, "Application of two-stage learning on brain-like system," in *Proc. IEEE Int. Conf. Neural Netw.Brain*, Beijing, China, Oct. 2005, vol. 3, pp. 1580–1584.
[7]D. M. Skapura, *Building Neural Networks*. Reading, MA, USA: Addison-Wesley, 1996.
[8]C.-T. Lin and C. S. G. Lee, *Neural Fuzzy Systems: A Neuro-Fuzzy Synergism to Intelligent Systems*. Englewood Cliffs, NJ, USA: Prentice-Hall, 1996.
[9]H. Dmathur and S. Ghosh, "A comprehensive analysis of intelligent controllers for load frequency control," in *Proc. IEEE Power India Conf.*, 2006, p. 5.
[10]D. Driankov, H. Hellendoorn, andM. Reinfrank, *An Introduction to Fuzzy Control*, 2nd ed. Berlin, Germany: Springer-Verlag, 1996.
[11]F. Zidani and R. N. Saúd, "Direct torque control of induction motor with fuzzy minimization torque ripple," *J. Elect. Eng.*, vol. 56, no. 7/8, pp. 183–188, 2005.
[12]H. Halleh, M. Rahmani, and B. Kimiaghalam, "Direct torque control of induction motors with fuzzy logic controller," in *Proc. IEEE Conf. Control, Autom. Syst.*, Seoul, Korea, Oct. 14–17, 2008, pp. 345–350.
[13]L. Youb and A. Craciunescu, "Direct torque control of induction motors with fuzzy minimization torque ripple," in *Proc. WESCO*, 2009, vol. 2, pp. 713–717.
[14]Y. V. S. Reddy, M. Vijayakumar, and T. B. Reddy, "Direct torque control of induction motor using sophisticated lookup tables based on neural networks," *AIML J.*, vol. 7, no. 1, pp. 9–15, Jun. 2007.
[15]J.-K. Kang, D.-W. Chung, and S.-K. Sul, "Direct torque control of induction machine with variable amplitude control of flux and torque hysteresis bands," in *Proc. IEMDC*, 1999, pp. 640–642.